Estimation of Dynamic Stress Intensity for One-Point Bend Specimen by Inverse Analysis*

Fergyanto E. GUNAWAN**, Hiroomi HOMMA**,
Qashim H. SHAH*** and Sandro MIHRADI****

The inverse method applied successfully to several basic structures is extended to estimate dynamic stress intensity-time history for one point bend specimens. The response functions of the specimens are estimated by de-convolving the specimen response measured near the crack tip with the measured impact force. Two methods of deconvolution were used, e.g., a simple statistical method and a CG-FFT iteration method. The ill-posed nature of the deconvolution is removed successfully by the CG-FFT method and then the excellent estimation is obtained.

Key Words: Inverse Problem, One-Point Bend Specimen, CG-FFT, Stress Intensity Factor

1. Introduction

The inverse methods have been developed and widely applied to scientific and engineering problems. In the field problems, the methods are classified as[1]:

- Domain/boundary inverse problems,
- Governing equation inverse problems,
- Boundary value/initial value inverse problems,
- Force inverse problems, and
- Material properties inverse problems.

The term of the inverse problem is not well defined yet, but most of the researchers, define the inverse problem as contrast with the direct problem[1),(2)]. In the direct problem, an unknown variable is output and known variables are input and system parameters.

In the inverse problem, the unknown variables may be input or system parameters. In many engineering problems, basic driving force to develop the inverse analysis is inability or inaccuracy in direct measurement of quantities under interest. In those circumstances, the quantities are inferred from others quantities, which are easily measured. For example, impact force is estimated by recorded response of the impacted structure, if the structure response function in known.

In this paper, the inverse analysis is employed to overcome the difficulties of strain-gage method that will be mentioned in the next part in determination of stress intensity factor. The inverse method is applied to identify the response function of the impacted specimen and estimate the dynamic stress intensity. Thus this work can be categorized into the initial value inverse problem.

2. Definition and Property of Problem

2.1 Dynamic stress intensity measurement

The fracture mechanics has been matured for recent years. Fracture mechanics parameters such as static and dynamic fracture toughness become important parameters in designing any engineering structure. In the dynamic fracture experiment, the stress intensity factor can be measured using optical method

* Received 24th October, 2001
** Department of Mechanical Engineering, Toyohashi University of Technology, 1-1 Hibarigaoka, Tempaku, Toyohashi 441-8580, Japan. E-mail: gunawan@mech.tut.ac.jp E-mail: homma@icceed.tut.ac.jp
*** Department of Mechanical Engineering, International Islamic University, Jalan Gombak 53100 KL, Malaysia
**** Department of Aeronautical Engineering, Bandung Institute of Technology, Ganesa 10, Bandung 40132, Indonesia

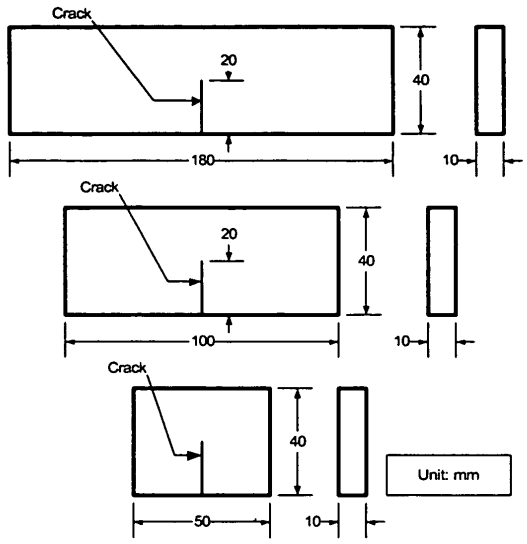

Fig. 1 Three types of one-point bend specimens

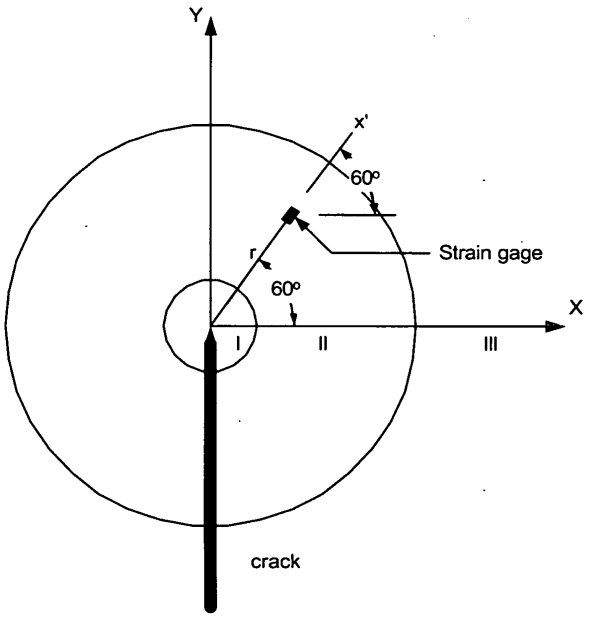

Fig. 2 The position and orientation of the strain gage in dynamic stress intensity measurement

or electrical strain gage.

The measurement of a dynamic stress intensity factor using strain gage proposed by Dally and Sanford[3] has been established on one-point bend specimen. The three types of one-point bend specimens depicted in Fig. 1 have been used for studying fracture mechanisms under impulsive stress intensity loading and dynamic fracture toughness[4]. The strain gage is attached at the particular distance and in the particular orientation from the crack tip as shown in Fig. 2. Strain recorded by the gage is converted into a dynamic stress intensity factor by the following formula[3]:

$$K_{Id}=E\sqrt{\frac{8}{3}\pi r}\,\epsilon_{x'x'} \qquad (1)$$

where $\epsilon_{x'x'}$ is strain in x' direction. The problem arising in this method is that; the size of the strain gage, which is relatively small (in order of 1 - 2 mm) makes trouble in the attachment of the strain gage concerning the accurate position and accurate orientation, and also a strain gage must be mount on each specimen to measure dynamic stress intensity. It takes long time to prepare the specimen. If the inverse analysis method is applied to measurement of the dynamic stress intensity the problems mentioned above can be solved.

In the linear elastic fracture mechanics, a linear relationship is held between impact force and response of the specimen. Based on this assumption, the response of specimen (for example in the gage position) can be inferred from measurement of impact force. In this research, a new method to estimate the response of a structure at the crack tip region, dynamic stress intensity measurement, is proposed on the bases of inverse analysis techniques.

2.2 Ill-posed numerical analysis in inverse problem

The inverse analysis has been applied to very wide engineering problems in the last decade. Some examples of inverse analysis in engineering problems are reconstruction of unknown force, reconstruction of signals, image reconstruction, tumor identification in medicine, optical topography, and system identification.

For a linear system, response of the structure subject to the impact force is expressed by a convolution equation in the form as:

$$u(t)=\int_0^t h(t-\tau)p(\tau)d\tau \qquad (2)$$

where, $u(t)$ is a vector of the response of the structure (in this case is the strain ahead of the crack tip), $h(t)$ is a vector of an impulse response function, $p(t)$ is the impact force vector.

The convolution integral form of Eq.(2) can be simplified by application of the convolution theorem by which the time domain convolution is rewritten into a simple multiplication form in Laplace image domain or Fourier image domain. In Eq.(2), the response at the crack tip $u(t)$ can be inferred from $p(t)$ if the response function $h(t)$ is given. The impulse response function can be estimated by means of numerical analysis or a calibration test. The equation for impulse response function obtained by rearranging of Eq.(2) as,

$$\hat{H}(s)=\frac{\hat{U}(s)}{\hat{P}(s)} \qquad (3)$$

where upper case parameters with hat means Laplace

transform of lower case in time domain.

Hadamard[2] showed that the mathematical formula become ill-posed if it has:

- No solution,
- Ambiguity, and
- Instability.

In Eq.(3), the impact force $\hat{P}(s)$ normally has limited bandwidth, but in reality noise always exists on a signal. Thus high frequency small randomly distributed noise is contaminated on the signal. Theoretically, if $\hat{U}(s)$ is zero at a particular frequency, the $\hat{P}(s)$ should be zero at that frequency. However in the deconvolution of Eq.(2) or Laplace transformed domain division of Eq.(3), the small noise in $\hat{P}(s)$ will blow up and make the deconvolution unstable. The problem becomes ill-posed under Hadamard's third condition.

3. Problem Solution

3.1 Solution for dynamic stress intensity by means of inverse analysis

As stated in the previous section, the response ahead of the crack tip can be inferred by measurement of the impact force applied on the specimen. The procedures to estimate response of the one-point bend specimen can be summarized as:

- A calibration experiment or numerical analysis is conducted in order to determine the impulse response function $h(t)$. In this paper, the impulse response function is determined using calibration experiment.
- The response function is identified by Eq.(3) or a robust iterative method, which will be explained in the next section.
- The specimen is subjected to a particular load-time history and then the load history is recorded.
- Using the estimated response function and the impact load history, the response ahead of the crack tip can be estimated by Eq.(2).

3.2 Solution for ill-posed deconvolution problem

Two methods of the deconvolution are used in this research. They are:

- Statistical method, and
- Iterative method.

In the statistical method, the ill conditioning of the deconvolution caused by noise is reduced on the basis of statistical principle. The variance of noise should decrease with increase of the number of experiments, and then the Eq.(3) are modified for a set of experiments as:

$$\hat{H}(s)=\frac{\sum \hat{U}(s)}{\sum \hat{P}(s)} \qquad (4)$$

In the iterative method, the Conjugate Gradient method and Fast Fourier transform (CG-FFT) are joined. Instead of solving the deconvolution directly, the convolution problem is formulated into a functional form as:

$$e(t)=u(t)-\int_0^t h(t-\tau)p(\tau)d\tau \qquad (5)$$

Using Eq.(5), the convolution problem is transformed into minimization of functional error $e(t)$. The solution procedures are summarized as follows:

Initialize Stage

- Assume an initial impulse response function h_0
- Calculate error vector

$$e(t)=u(t)-\int h_0(t-\tau)p(\tau)d\tau$$

- Calculate search vector

$$p_1=-\int[p(t-\tau)]^{\perp}e(t)d\tau$$

Iteration ($n=1\,2,\cdots$)

- Update step

$$\alpha_n=\frac{\left\|\int[p(t-\tau)]^{\perp}e_{n-1}(t)d\tau\right\|^2}{\|p(t-\tau)p_n(\tau)d\tau\|^2}$$

- Update $h(t)$

$$h_n=h_{n-1}+\alpha_n p_n$$

- Update error vector

$$e_n=u(t)-\int h_n(t-\tau)p(\tau)d\tau$$

Note: $[\diamond]^{\perp}$=Conjugate transposition, $\|\diamond\|$=Euclidean vector norm.

The calculation of convolution and advanced convolution integration can be speeded up by the FFT. The Euclidean norm of error vector $e(t)$ physically means the distance between the measured structural response and the estimated structural response, which is computed using the estimated response function. The norm of the error vector is a parameter to terminate the iteration.

4. Experimental Setup and Loading Cases

The experimental apparatus is schematically depicted in Fig. 3. The magnitude of impact force is controlled by the pressure of Nitrogen gas (N_2) that accelerates the projectile. The contact duration at collision between the projectile and the load transfer rod does not change significantly with pressure of N_2 gas. To prepare the different contact duration, two different lengths of projectiles are used. Two strain gages are attached at the load transfer rod in half bridge configuration in order to eliminate the bending deformation induced by the tint collision. A semicon-

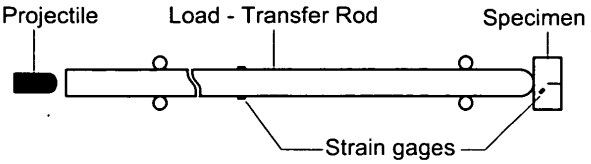

Fig. 3 The Experimental apparatus

Table 1 Experimental conditions

Load Case	Projectile (mm)	Pressure (kg/mm^2)
For 50mm length of specimen		
Case 1	25	0.8
Case 2	25	0.5
Case 3	50	0.5
For 100mm length of specimen		
Case 1	25	0.5
Case 2	25	0.8
For 180mm length of specimen		
Case 1	50	0.8
Case 2	25	0.5
Case 3	25	0.8

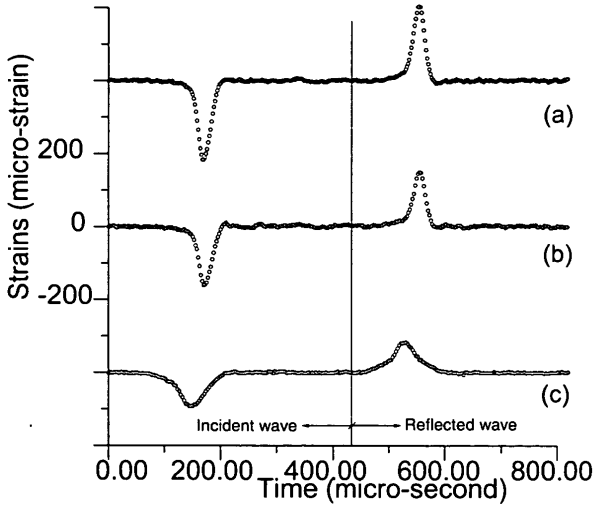

Fig. 4 Incident and reflected waves on the load transfer rod in 50 mm long specimen; (a) load case 1; (b) load case 2; (c) load case 3

ductor strain gage is mounted on the specimen. That gage has a gage factor up to 126, around 60 times higher than a common strain gage. The around 9000 data are recorded from each strain gage with sampling time of 0.1 μ-second.

The type of the specimen and experimental conditions are summarized in Table 1, and the geometry of specimen is depicted in Fig. 1.

5. Experimental Results

The data recorded by the gages at the load transfer rod and specimens for all the load cases are shown in Figs. 4 - 9. As seen in Figs. 5, 7, and 9, all the vibrations are dominated by the first natural frequency of the specimen. Some high frequency vibration modes are superimposed on the vibration of the 180 mm long specimen. The natural frequency decreases as the specimen length increases from 50 mm to 180 mm. In Figs. 4 and 8, the contact duration of a 50 mm projectile is longer than a 25 mm projectile

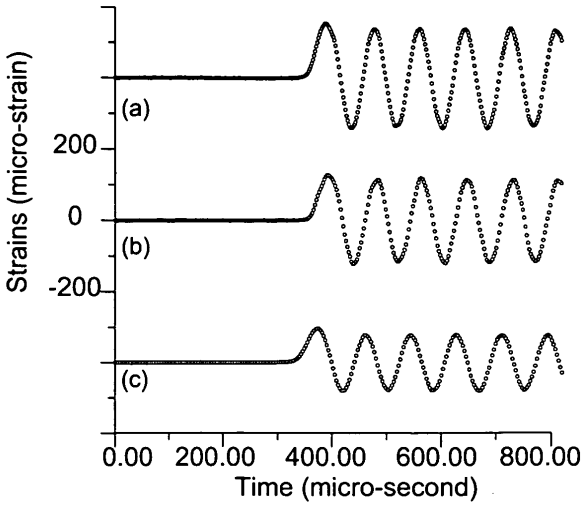

Fig. 5 Response of 50 mm long specimen; (a) load case 1; (b) load case 2; (c) load case 3

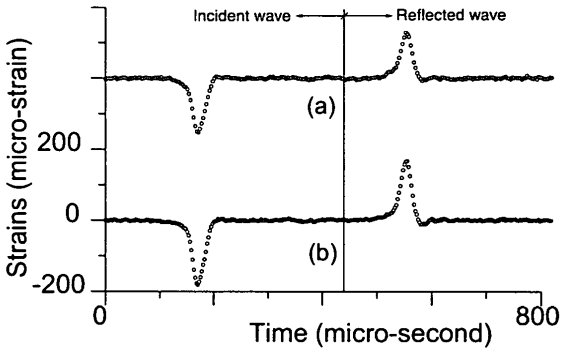

Fig. 6 Incident and reflected waves measured on the load transfer rod in 100 mm long specimen; (a) load case 1; (b) load case 2

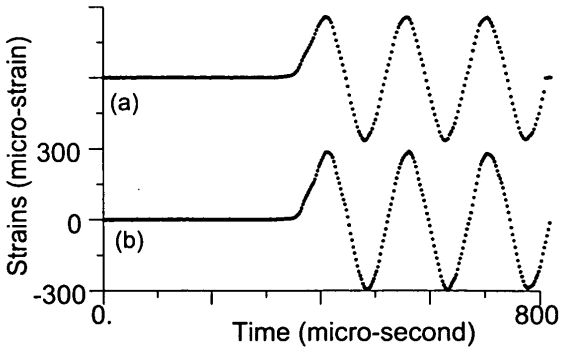

Fig. 7 Response of 100 mm long specimen; (a) load case 1; (b) load case 2

as expected. Also in those figures, the absolute magnitude of the incident wave is higher than the reflected wave. The magnitude of a transmitted wave into the specimen is calculated as:

$$|p_{trans}|_{max}=|p_{incident}|_{max}-|p_{reflected}|_{max} \quad (6)$$

The profile of the transmitted wave is assumed similar with the incident wave. The semi-conductor gages have shown their excellent performance in

Table 2 The cross-checking evaluation

Case	Data	Estimated $h(t)$	Applied for
1	u_1		$\hat{u}_2 = h_1 * p_2$
		$\rangle \rightarrow h_1 \rightarrow \langle$	
	p_1		$\hat{u}_3 = h_1 * p_3$
2	u_2		$\hat{u}_1 = h_2 * p_1$
		$\rangle \rightarrow h_2 \rightarrow \langle$	
	p_2		$\hat{u}_3 = h_2 * p_3$
3	u_3		$\hat{u}_2 = h_3 * p_2$
		$\rangle \rightarrow h_3 \rightarrow \langle$	
	p_3		$\hat{u}_1 = h_3 * p_1$

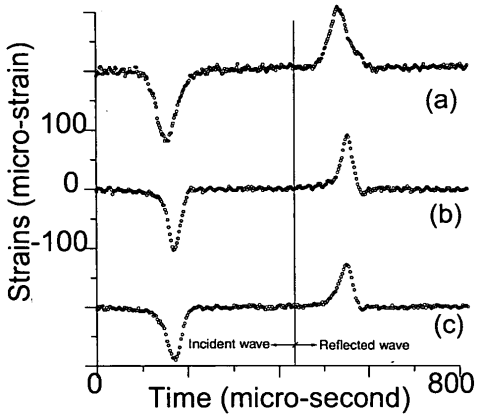

Fig. 8 Incident and reflected waves measured on the load transfer rod for 180 mm long specimen; (a) load case 1; (b) load case 2; (c) load case 3

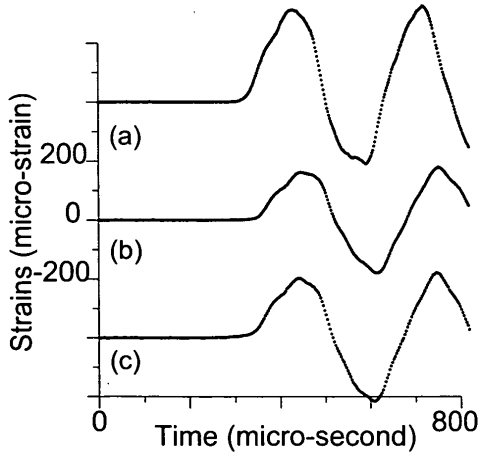

Fig. 9 Response of 180 mm long specimen; (a) load case 1; (b) load case 2; (c) load case 3

noise reduction over the common strain gages. This is clear by comparing the strain-time history at the rod in Fig. 8, which is measured using common strain gages, with the strain-time history at the specimen in Fig. 9. Before the projectile collides with the load transfer rod, the semi-conductor gage output displays almost constant zero strain.

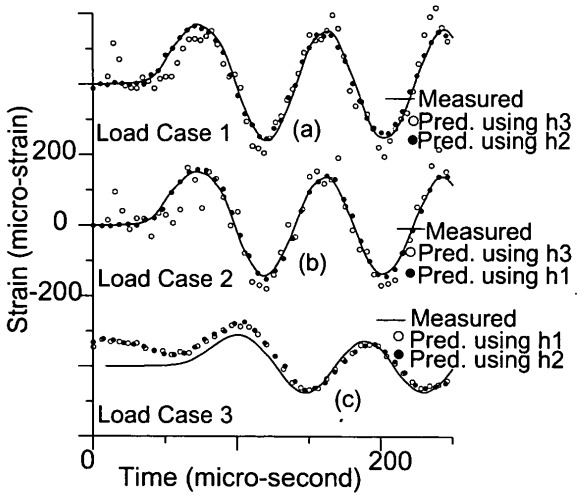

Fig. 10 Prediction for 50 mm length specimen using simple statistical method; (a) $h(t)$ from load cases 2 and 3; (b) $h(t)$ from load cases 1 and 3; (c) $h(t)$ from load cases 2 and 3

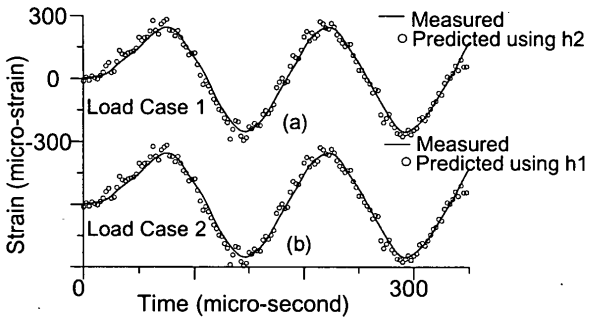

Fig. 11 Prediction for 100 mm length specimen using simple statistical method; (a) $h(t)$ from load case 2; (b) $h(t)$ from load case 1

6. Results and Discussion

In order to examine the performance of inverse analysis, the experiments are conducted to obtained calibration results. For the load cases and the specimens summarized in Table 1, the impact force and the response ahead of the crack tip are measured. In the 50 mm long specimen, the response function is estimated using the data from three load cases. The scheme of cross checking evaluation is explained in Table 2, where $\hat{u}_i(t)$ for $i=1, 2, 3$ is an estimated response of the structure, and the subscript i indicates the load case, for instance $i=1$ means the load case 1. The similar cross checking evaluations are carried out for the 100 mm and the 180 mm long specimen.

The prediction results of the response of the one-point bend specimen are shown in Figs. 10 to 12 for the simple statistical deconvolution and in Figs. 13 to 15 for the deconvolution solved by the Conjugate Gradient-FFT iteration method.

In the CG-FFT scheme, the iteration are ter-

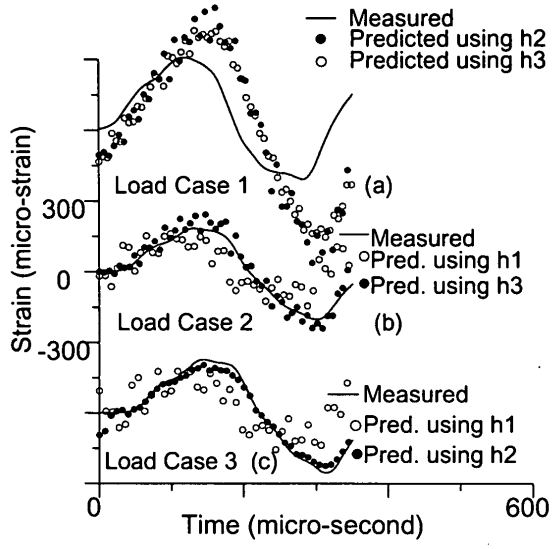

Fig. 12 Prediction for 180 mm length specimen using simple statistical method; (a) $h(t)$ from load cases 2 and 3; (b) $h(t)$ from load cases 1 and 3; (c) $h(t)$ from load cases 2 and 3

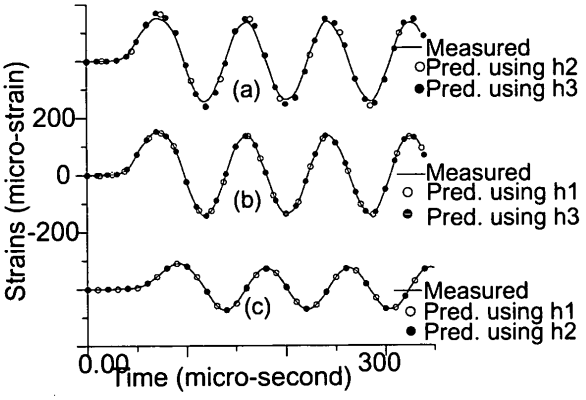

Fig. 13 Prediction for 50 mm length specimen using CG-FFT method; (a) $h(t)$ from load cases 2 and 3; (b) $h(t)$ from load cases 1 and 3; (c) $h(t)$ from load cases 2 and 3

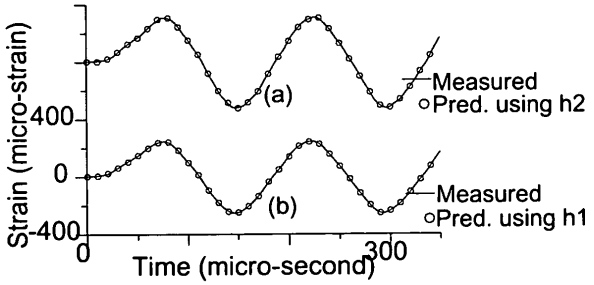

Fig. 14 Prediction for 100 mm length specimen using CG-FFT method; (a) $h(t)$ from load case 2; (b) $h(t)$ from load case 1

minated if the iteration number reaches 1.E+5 or a Euclidean norm of residual vector decreases to smaller than 1. E-3. From the observation of Figs. 10 to 15 the following facts are deduced:

Table 3 The CG-FFT computation summary

Processor	Alpha workstation 500MHz
OS Env.	Tru64 UNIX
Flops	3.2074E+11⊕
Comp. time	± 13 hours⊕
Error history	(see Fig. 16)

Note: ⊕ is based on floating point operation (flops) and computing time for 50mm long specimen under three load cases. The rate of convergence is strongly depending on initialization of transfer function $h(t)$, the initial transfer function $h_0(t)$ is assumed as a unit step function.

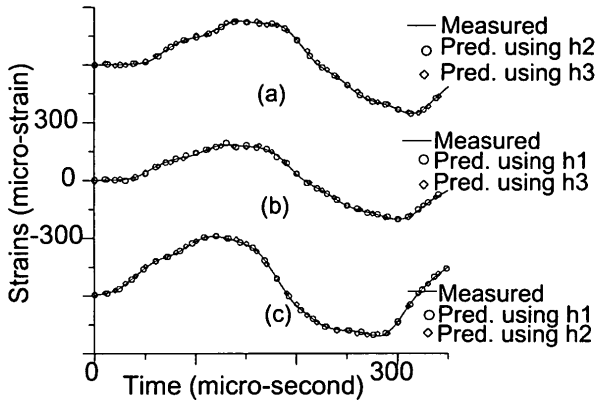

Fig. 15 Prediction for 180 mm length specimen using CG-FFT method; (a) $h(t)$ from load cases 2 and 3; (b) $h(t)$ from load cases 1 and 3; (c) $h(t)$ from load cases 2 and 3

• The simple deconvolution formula (Eq.(4)) gives relatively poor prediction if the predicted load case is very different from the load case where the response function is estimated.

• Figures 10 to 12 show that the influence of the noise on the estimated structural response is significant. The noise in the load transfer rod tends to expand up after conducting the division. The placement of common strain gage at the load transfer rod does not seem to be a good choice by referring to the Eq.(3) where the denominator is strain at the load transfer rod.

• The estimation using the CG-FFT method gives excellent agreement with measured structural response.

7. Conclusions

New methods of dynamic stress intensity measurement based on the inverse analysis are examined. The method based on the CG-FFT has two advantages compared with the previous method[4]; the first is reduction of the number of strain gages and the second is minimization of the measurement error caused by improper location and orientation of a gage. The disadvantage of this method is that the robust

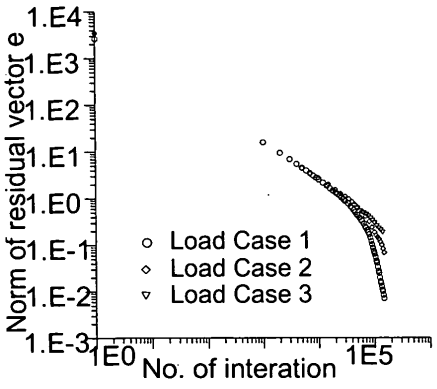

Fig. 16 Convergence of the norm of residual vector—the number iterations are terminated after 1.0E+5—for three load cases of 50 mm specimen

computational method of the response function is relatively expensive, but once the response function for a particular geometry and material has been determined, the cost will be reduced significantly for other experiments.

References

(1) Kubo, S., Classification of Inverse Problems Arising in Field Problems and Their Treatments, (Edited by M. Tanaka and H.D. Bui), IUTAM Symposium Tokyo/Japan (1993), pp. 51-60, Springer-Verlag, Berlin.

(2) Baumeister, J., Stable Solution of Inverse Problems, (1987), Friedr. Vieweg & Sohn.

(3) Dally J.W. and Sanford R.J., Strain-Gage Methods for Measuring the Opening-Mode Stress-Intensity Factor KIC, Experimental Mechanics, Vol. 27 (1987), pp. 381-388.

(4) Rizal, S. and Homma, H., Dimple Fracture under Short Pulse Loading, International Journal of Impact Engineering, Vol. 24 (2000), pp. 69-83.

(5) Peterson Andrew, F., Ray Scott, L. and Mittra, R., Computation Methods for Electromagnetic, (1960), pp. 161-179, IEEE Press, New York.

(6) Golub, G.H. and Van Loan, C.F., Matrix Computations, (1989), pp. 505-538, The Johns Hopkins University Press, London.

(7) Young, Iterative Solution of Large Linear System, (1971), Academic Press, USA.